Chinese Physics B

PAPER

Antiferromagnetic interlayer coupling of (111)-oriented $La_{0.67}Sr_{0.33}MnO_3/SrRuO_3$ superlattices*

Antiferromagnetic interlayer coupling of (111)-oriented $La_{0.67}Sr_{0.33}MnO_3/SrRuO_3$ superlattices*

Hui Zhang(张慧)[1,2], Jing Zhang(张静)[1,2], Jin-E Zhang(张金娥)[1,2], Fu-Rong Han(韩福荣)[1,2], Hai-Lin Huang(黄海林)[1,2], Jing-Hua Song(宋京华)[1,2], Bao-Gen Shen(沈保根)[1,2], and Ji-Rong Sun(孙继荣)[1,2,†]

[1] *Beijing National Laboratory for Condensed Matter Physics, Institute of Physics, Chinese Academy of Sciences, Beijing* 100190, *China*
[2] *School of Physical Sciences, University of Chinese Academy of Sciences, Beijing* 100049, *China*

(Received 27 November 2018; revised manuscript received 25 December 2018; published online 23 January 2019)

We report a strong antiferromagnetic (AFM) interlayer coupling in ferromagnetic $La_{0.67}Sr_{0.33}MnO_3/SrRuO_3$ (LSMO/SRO) superlattices grown on (111)-oriented $SrTiO_3$ substrate. Unlike the (001) superlattices for which the spin alignment between LSMO and SRO is antiparallel in the in-plane direction and parallel in the out-of-plane direction, the antiparallel alignment is observed along both the in-plane and out-of-plane directions in the present sample. The low temperature hysteresis loop demonstrates two-step magnetic processes, indicating the coexistence of magnetically soft and hard components. Moreover, an inverted hysteresis loop was observed. Exchange bias tuned by the temperature and cooling field was also investigated, and positive as well as negative exchange bias was observed at the same temperature with the variation of the cooling field. A very large exchange field ($\boldsymbol{H}_{\rm EB}$) was observed and both magnitude and sign of the $\boldsymbol{H}_{\rm EB}$ depend on the cooling field, which can be attributed to an interplay of Zeeman energy and AFM coupling energy at the interfaces. The present work shows the great potential of tuning a spin texture through interfacial engineering for the complex oxides whose spin state is jointly determined by strongly competing mechanisms.

Keywords: transition metal oxide, interlayer coupling, exchange bias

PACS: 75.47.Lx, 75.70.Cn, 75.25.–j **DOI:** 10.1088/1674-1056/28/3/037501

1. Introduction

Complex oxide interfaces have attracted extensive attention owing to the emergent phenomena that are absent in bulk materials, such as the two-dimensional electron gas (2DEG) between two band insulators,[1–3] ferromagnetism in superlattices composed of two antiferromagnets,[4] and the exchange coupling at the paramagnet/ferromagnet interfaces.[5] Obviously, interface engineering offers valuable opportunities for manipulating the properties of complex oxide artificial materials, via interfacial symmetry breaking, epitaxial strains, octahedral rotation, charge transfer, etc.[6–12] In particular, the magnetic interlayer coupling is very interesting in the sense that it provides an approach to tailor and tune the interfacial spin structure, which is the central issue of spintronics.

Among oxide interfaces, the manganite/ruthenate interface is a model system for the investigation of interfacial effects. One of the intensively studied systems is (001)-oriented $La_{0.67}Sr_{0.33}MnO_3/SrRuO_3$ (LSMO/SRO). Ke *et al.* first reported a positive exchange bias effect in LSMO/SRO bilayers.[13,14] Soon after that, Ziese *et al.* presented a systematic investigation of the LSMO/SRO superlattices grown on (001)-oriented $SrTiO_3$ (STO), and reported a strong antiferromagnetic (AFM) interlayer coupling and an inverted hysteresis loop.[15,16] Thota *et al.* observed a crossover from the conventional to the inverse magnetocaloric effect.[17] Meanwhile, a switching from ferromagnetic (FM) to AFM interlayer coupling was observed in the (001) superlattices when changing the applied field from the out-of-plane to the in-plane directions.[18]

In those works, attention was focused mainly on the (001)-oriented LSMO/SRO system. However, physical properties are strongly dependent on the oriented substrate. For example, $Nd_{0.5}Sr_{0.5}MnO_3$ thin films deposited on (001), (110), and (111)-oriented STO substrates have different charge- and orbital-ordered states.[19,20] Moreover, the FM order of thin films/superlattices of perovskite manganites will be strongly depressed by the interface/surface for (001) films due to lattice strains or the presence of a magnetic dead layer. In contrast, an enhanced magnetization has been reported for the SRO films grown on (111)-oriented STO.[21] Compared with (001) films, the interfacial states in (111) multilayers could be completely different, and thus deserve special attention. We notice that works in this regard are scarce. The only research was conducted by Behera *et al.*,[22] who presented an investigation into the Raman spectra of the (111) LSMO/SRO superlattices on STO, and suggested a variation of the stereochemistry of Mn at the interfaces. However, the magnetic characteristics were not revealed there. In this paper, we report an investigation of the magnetic properties of the (111) LSMO/SRO superlattices grown on STO. We observed AFM interlayer coupling and

*Project supported by the National Basic Research Program of China (Grant Nos. 2016YFA0300701, 2017YFA0206300, and 2017YFA0303601) and the National Natural Science Foundation of China (Grant Nos. 11520101002, 51590880, and 11674378).

†Corresponding author. E-mail: jrsun@iphy.ac.cn

dual exchange bias phenomena, a consequence of the competition between Zeeman energy and interfacial coupling energy. The results demonstrate that the (111)-oriented LSMO/SRO superlattices could be a model system for the investigation of interfacial exchange coupling in functional oxides.

2. Experiments

Superlattices with alternately stacked SRO and LSMO layers were grown using the technique of pulsed laser deposition (PLD) with a 248 nm KrF excimer laser on (111)-oriented STO single crystal substrates (4 mm×4 mm×0.5 mm). The repetition rate was 2 Hz and the laser fluence was 2 J/cm^2. During deposition, the substrate temperature was maintained at 600 °C (for SRO) or 700 °C (for LSMO), and the oxygen pressure was fixed to a constant value of 30 Pa. After deposition, the sample was furnace-cooled to room temperature in an oxygen atmosphere of 100 Pa. The layer thickness was determined by the number of laser pulses, which had been carefully calibrated using the technique of small angle x-ray reflectivity (XRR). Here we focus on the LSMO/SRO superlattices with a periodicity of 4, and the layer thickness is 6 nm for LSMO and 8 nm for SRO. The crystal structure of the superlattices was determined by a Bruker x-ray diffractometer equipped with thin film accessories (D8 Discover, Cu K_α radiation). Magnetic measurements were performed on the Quantum Design vibrating sample magnetometer (VSM-SQUID).

3. Results and discussion

As an example, we show the small-angle XRR result for a single SRO/STO(111) film in Fig. 1(a). The regular and periodic oscillation indicates a smooth film surface and a homogeneous film thickness. Using fast Fourier transition fitting, the layer thickness can be determined, and it is 16.3 ± 0.4 nm. From the deposition time, we obtain the growth rate of SRO. For the LSMO layer, the deposition rate is determined in the same way. Figure 1(b) is a schematic diagram of the LSMO/SRO superlattices fabricated on (111)-oriented STO substrate. Figure 1(c) presents the x-ray diffraction (XRD) spectra of superlattices. Besides the main (111) reflection of the substrates, satellite peaks corresponding to the superlattice structure (marked by the numbers above the corresponding peaks) and the finite-size oscillations (marked by triangles) can be clearly seen, signaling the high quality of the specimen. According to the Bragg diffraction equation ($2d\sin\theta = n\lambda$), the out-of-plane lattice parameter d_{111} of the superlattices can be calculated from the zeroth order satellite peak position, and it is 2.2618 Å. This value is slightly larger than that of the STO substrate (2.2542 Å), indicating that the LSMO/SRO superlattice is slightly in-plane compressive or, equivalently, out-of-plane tensile.

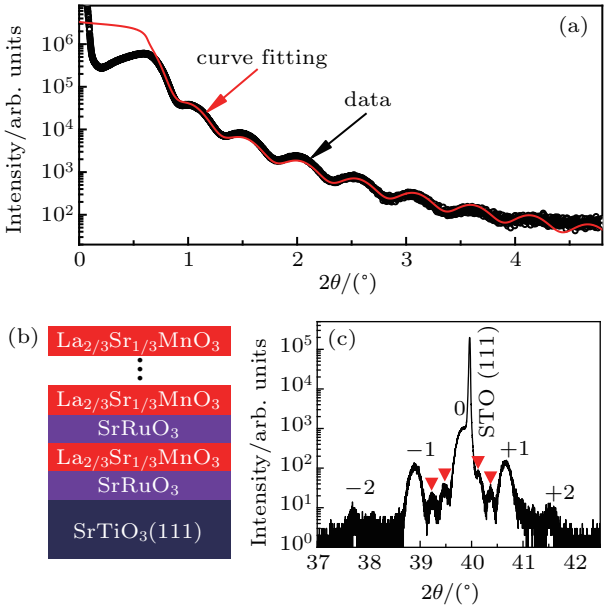

Fig. 1. (a) Small angle x-ray reflectivity of the SRO single layer (symbols) and the corresponding result of data fitting (red curve) that gives a layer thickness of 16.3 ± 0.4 nm. (b) A sketch of the LSMO/SRO superlattices grown on (111)-oriented STO substrate. (c) XRD patterns of the superlattices.

Figure 2 displays the temperature-dependent in-plane and out-of-plane magnetization measured under different applied fields in field-cooling mode. Two magnetic transitions are clearly seen. The first one, which takes place at ∼ 320 K, is a paramagnetic-to-ferromagnetic transition of the LSMO layers. The Curie temperature (T_C) is relatively smaller than that of bulk LSMO.[23,24] As shown in Fig. 2(a), when the superlattice is cooled below ∼ 320 K, the magnetization first increases rapidly, and then gradually increases when the temperature is much lower than T_C. This is the typical behavior of the LSMO. When the temperature sweeps through ∼ 160 K, the SRO layers become ferromagnetic, and an intriguing phenomenon emerges. The contribution from SRO undergoes a systematic variation with the increase of the applied fields. Under low fields, the magnetic transition of SRO leads to a cusp at 160 K in the M–T curve and a subsequent slow decrease in magnetic moments upon further cooling. This decrease is a signature of the AFM exchange coupling between LSMO and SRO. In higher fields, $H \geq 1$ T, the magnetic moments of the LSMO and SRO layers gradually rotate toward the field direction. As a result, the magnetic change below ∼ 160 K evolves gradually from decrease to increase as the cooling field grows. This field-induced spin flip is also observed in Fig. 2(b) when applying perpendicular fields, showing that it is not due to spin reorientation. Notably, the magnetic moments of the LSMO and SRO layers are always antiparallel to each other when the applied fields are low, regardless of whether the fields are in-plane or out-of-plane. This is in sharp contrast to (001) superlattices, for which the magnetic moments of the LSMO and SRO layer align in parallel when measured with perpendicular fields and in antiparallel when measured using in-plane fields.

It is noted that in low fields, the magnetic moments are significantly larger when measured with in-plane fields than with out-of-plane fields, indicating that the magnetic hard axis is along the film normal. Therefore, in the following study we focus on in-plane magnetization.

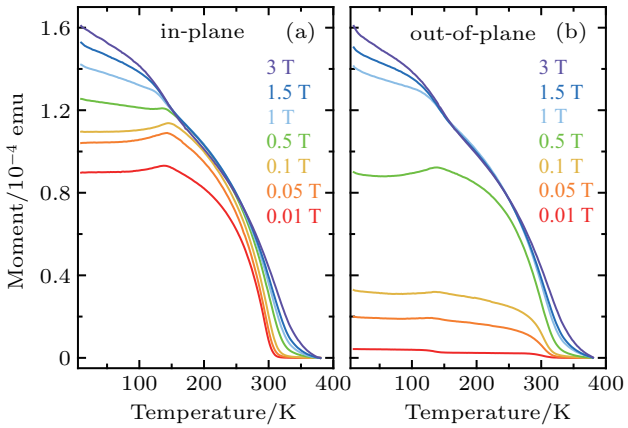

Fig. 2. The field-cooled magnetization of the (111)-oriented LSMO/SRO superlattices under various magnetic fields as a function of temperature. Magnetic fields were applied (a) parallel and (b) perpendicular to the superlattices respectively.

As shown in Fig. 3, the magnetic hysteresis loop recorded at 10 K indicates the coexistence of a soft and a hard magnetic phase, as demonstrated by the appearance of two-step magnetizing behaviors characterized by wasp-waisted magnetic curves. The thin elongated wasp-waist is ascribed to LSMO, and the other two waists to SRO, because the coercive field of SRO is much larger than that of LSMO. The most prominent feature of the hysteresis curves is the inversion of the central part of the magnetic loop. Since the magnetic moment of LSMO ($\sim 3.7\ \mu_B$/Mn) is larger than that of SRO ($\sim 1.6\ \mu_B$/Ru), the LSMO layer dominates the magnetic behavior of the superlattices. Different from LSMO, SRO has a strong magneto-crystalline anisotropy at low temperatures. Starting at a high positive field which is large enough to align the magnetic moments of all layers in the positive direction, the SRO magnetization will remain unchanged as the applied field decreases due to its strong anisotropy, but the LSMO layer will experience a magnetic reversal. Without interlayer exchange at the interface, this reversal occurs at zero field. However, due to the AFM interfacial exchange, the LSMO layers reverse their magnetization in finite positive fields before the reversal of the hard SRO layers at high negative fields. As a consequence, an inverted hysteresis loop appears.

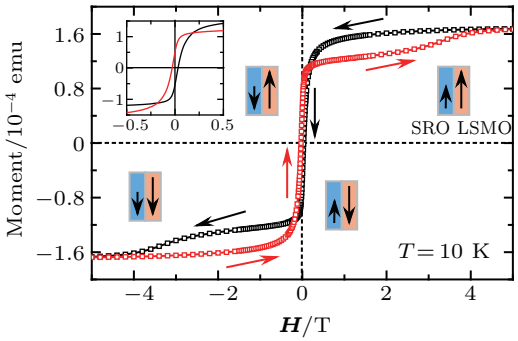

Fig. 3. Field dependence of the magnetic moment recorded at 10 K with in-plane fields. The arrows indicate the field sweep direction. The relative layer magnetic orientation is illustrated in the inset diagrams. The inset curve shows a close-up view of the central part of the magnetic loop.

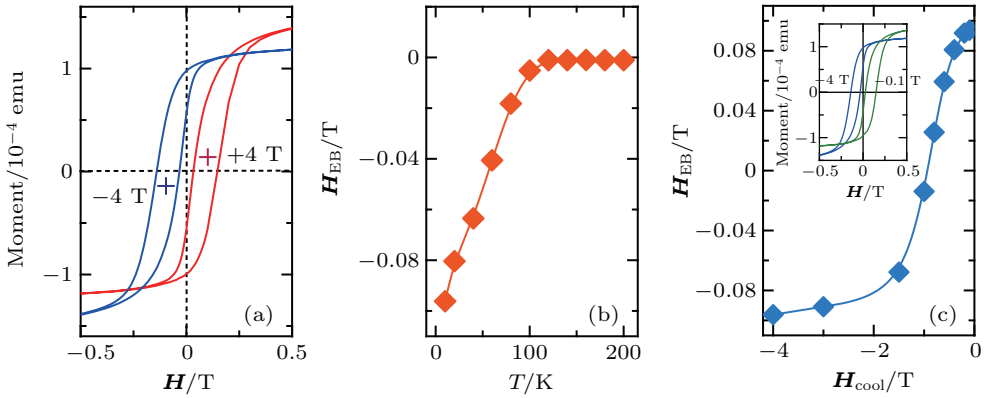

Fig. 4. (a) Minor loops at 10 K under cooling field $\boldsymbol{H}_{\rm cool} = \pm 4$ T for (111)-oriented LSMO/SRO superlattices. (b) The temperature dependence of $\boldsymbol{H}_{\rm EB}$ with $\boldsymbol{H}_{\rm cool} = -4$ T. (c) The cooling field dependence of $\boldsymbol{H}_{\rm EB}$ at $T = 10$ K. Inset shows the hysteresis loop with $\boldsymbol{H}_{\rm cool} = -4$ T and -0.1 T.

In general, exchange bias manifests itself as a hysteresis loop, which is broadened and shifted along the field axis when cooled below a blocking temperature in an external magnetic field. Therefore, the exchange field ($\boldsymbol{H}_{\rm EB}$) can be tuned with both the temperature and the cooling field ($\boldsymbol{H}_{\rm cool}$). In further research, we systematically study the exchange bias in (111)-oriented LSMO/SRO superlattices. In Fig. 4(a), we show the minor loops recorded by saturating the superlattices under in-plane cooling fields of ± 4 T and then sweeping the applied field over the range ± 0.5 T at a temperature of 10 K. We find an obvious upper right (lower left) shift of the magnetic loop after field-cooling in $+4$ T (-4 T), yielding a positive exchange bias in agreement with the AFM nature of the interlayer coupling. The exchange field $\boldsymbol{H}_{\rm EB}$ is defined by the center field of the minor loop. As denoted by a red cross mark, when $\boldsymbol{H}_{\rm cool} = +4$ T, the center of the minor loop deviates from

the origin by a very large exchange field $\boldsymbol{H}_{\rm EB} = 1013$ Oe. Figure 4(b) shows the temperature dependence of the exchange field $\boldsymbol{H}_{\rm EB}$ with $\boldsymbol{H}_{\rm cool} = -4$ T. The absolute value of $\boldsymbol{H}_{\rm EB}$ decreases quickly with increasing temperature and is zero when the temperature is above the $T_{\rm C}$ of SRO. Furthermore, we also investigate how the cooling field affects the exchange field at 10 K. As shown in the inset of Fig. 4(c), as previously mentioned, after a field-cooling in -4 T, the hysteresis loop is shifted along the negative field axis. Surprisingly, the hysteresis loop is shifted along the positive field axis when cooling the superlattices with -0.1 T field, resulting in a negative exchange bias. Figure 4(c) shows the $\boldsymbol{H}_{\rm cool}$ dependence of the exchange field. For large negative cooling fields, the value of $\boldsymbol{H}_{\rm EB}$ is negative and nearly reaches saturation. With the decrease of the magnitude of $\boldsymbol{H}_{\rm cool}$, $\boldsymbol{H}_{\rm EB}$ changes sign, switching from negative to positive. Namely, dual exchange bias is obtained, i.e., either positive or negative exchange bias can be observed at the same temperature, depending on the cooling field.

Actually, both the magnitude and the sign of $\boldsymbol{H}_{\rm EB}$ depend on the cooling field, which can be attributed to the competition between Zeeman energy and AFM coupling energy at the interfaces. As the superlattices cool down to 10 K in the absence of a magnetic field, the magnetic moments of LSMO and SRO are aligned in antiparallel but their directions are random. However, during the field-cooling process, the LSMO layers first align with the cooling field (due to the in-plane easy axis of LSMO), while the SRO layers' alignment is determined by the competition between the Zeeman interaction with the external field and the exchange interaction with the LSMO layers. For large negative cooling fields, the Zeeman energy dominates over the interfacial coupling ($J_{\rm AF} < \boldsymbol{M} \cdot \boldsymbol{H}$), and thus the spins of the SRO layers rotate toward the magnetic field, but against the AFM coupling. Thus, during the magnetization reversal of the LSMO layers, it is easier to switch the LSMO layers to the positive direction than to the negative direction because of the AFM coupling with SRO. This causes the sign of the exchange field to be the same as that of the cooling field. Hence, a positive exchange bias is expected. While for small cooling fields, when interfacial coupling is larger than the dipole interaction on the SRO layer ($J_{\rm AF} > \boldsymbol{M} \cdot \boldsymbol{H}$), the interfacial SRO spins prefer to point in the direction opposite to the cooling field direction. In this case, when ramping magnetic field to a positive value, it is difficult to switch LSMO to the positive direction but relatively easy to switch LSMO back to the negative direction. This causes the sign of the exchange field to be opposite to that of the cooling field. Thus, a negative exchange bias is expected.

4. Summary

A strong AFM interlayer coupling in the LSMO/SRO superlattices grown on (111)-oriented STO substrate has been systematically studied. In sharp contrast to the in-plane AFM alignment and the out-of-plane FM alignment in (001) superlattices, our results indicate that the interlayer alignment is always antiparallel in (111)-oriented LSMO/SRO superlattices, independent of the direction of the applied fields. Magnetically soft and hard components are observed as being characterized by a two-step magnetizing behavior. Moreover, the inverted hysteresis loop is observed. Exchange bias in this artificial superlattice structure has also been investigated, which can be tuned by temperature and cooling field. We found that the presence of the dual exchange and both the magnitude and the sign of $\boldsymbol{H}_{\rm EB}$ depend on the cooling field, which can be attributed to the competition between Zeeman energy and interfacial coupling energy. The present work shows the great potential of interfacial engineering in designing artificial materials for both fundamental and applied research.

References

[1] Ohtomo A and Hwang H Y 2004 *Nature* **427** 423
[2] Nakagawa N, Hwang H Y and Muller D A 2006 *Nat. Mater.* **5** 204
[3] Herranz G, Basletic M, Bibes M, Carretero C, Tafra E, Jacquet E, Bouzehouane K, Deranlot C, Hamzic A, Broto J M, Barthelemy A and Fert A 2007 *Phys. Rev. Lett.* **98** 216803
[4] Ueda K, Tabata H and Kawai T 1998 *Science* **280** 1064
[5] Gibert M, Zubko P, Scherwitzl R, Iniguez J and Triscone J M 2012 *Nat. Mater.* **11** 195
[6] Sadoc A, Mercey B, Simon C, Grebille D, Prellier W and Lepetit M B 2010 *Phys. Rev. Lett.* **104** 046804
[7] Lu W, Song W, Yang P, Ding J, Chow G M and Chen J 2015 *Sci. Rep.* **5** 10245
[8] Chen Y Z, Trier F, Wijnands T, Green R J, Gauquelin N, Egoavil R, Christensen D V, Koster G, Huijben M, Bovet N, Macke S, He F, Sutarto R, Andersen N H, Sulpizio J A, Honig M, Prawiroatmodjo G E D K, Jespersen T S, Linderoth S, Ilani S, Verbeeck J, Van Tendeloo G, Rijnders G, Sawatzky G A and Pryds N 2015 *Nat. Mater.* **14** 801
[9] Liao Z, Huijben M, Zhong Z, Gauquelin N, Macke S, Green R J, Van Aert S, Verbeeck J, Van Tendeloo G, Held K, Sawatzky G A, Koster G and Rijnders G 2016 *Nat. Mater.* **15** 425
[10] Kan D, Aso R, Sato R, Haruta M, Kurata H and Shimakawa Y 2016 *Nat. Mater.* **15** 432
[11] Zhang J, Zhang H, Zhang X, Guan X, Shen X, Hong D, Zhang H, Liu B, Yu R, Shen B and Sun J 2017 *Nanoscale* **9** 3476
[12] Zhang J, Zhong Z, Guan X, Shen X, Zhang J, Han F, Zhang H, Zhang H, Yan X, Zhang Q, Gu L, Hu F, Yu R, Shen B and Sun J 2018 *Nat. Commun.* **9** 1923
[13] Ke X, Rzchowski M S, Belenky L J and Eom C B 2004 *Appl. Phys. Lett.* **84** 5458
[14] Ke X, Belenky L J, Eom C B and Rzchowski M S 2005 *J. Appl. Phys.* **97** 10K115
[15] Ziese M, Vrejoiu I, Pippel E, Esquinazi P, Hesse D, Etz C, Henk J, Ernst A, Maznichenko I V, Hergert W and Mertig I 2010 *Phys. Rev. Lett.* **104** 167203
[16] Ziese M, Vrejoiu I and Hesse D 2010 *Appl. Phys. Lett.* **97** 052504
[17] Thota S, Zhang Q, Guillou F, Lueders U, Barrier N, Prellier W, Wahl A and Padhan P 2010 *Appl. Phys. Lett.* **97** 112506
[18] Padhan P and Prellier W 2011 *Appl. Phys. Lett.* **99** 263108
[19] Nakamura M, Ogimoto Y, Tamaru H, Izumi M and Miyano K 2005 *Appl. Phys. Lett.* **86** 182504
[20] Wakabayashi Y, Bizen D, Nakao H, Murakami Y, Nakamura M, Ogimoto Y, Miyano K and Sawa H 2006 *Phys. Rev. Lett.* **96** 017202
[21] Grutter A, Wong F, Arenholz E, Liberati M, Vailionis A and Suzuki Y 2010 *Appl. Phys. Lett.* **96** 082509
[22] Behera B C, Padhan P and Prellier W 2016 *J. Phys.: Condens. Matter* **28** 196004
[23] Urushibara A, Moritomo Y, Arima T, Asamitsu A, Kido G and Tokura Y 1995 *Phys. Rev. B* **51** 14103
[24] Moritomo Y, Asamitsu A and Tokura Y 1995 *Phys. Rev. B* **51** 16491